# Active RCS Reduction in Series-fed Dipole Phased Array in Hostile Probing Environment

Adrija Chowdhury, Raveendrantah U. Nair, and Hema Singh*

*Centre for Electromagnetics (CEM),*CSIR-National Aerospace Laboratories, Bengaluru-560017, India
*hemasingh@nal.res.in*

**Abstract.** The radar cross section (RCS) of an aerospace platform can be reduced significantly by controlling the scattering from phased arrays mounted over it. This may be achieved by exploiting the capability of active cancellation of probing sources by the array. If the array reduces the RCS towards the hostile probing directions, the platform becomes invariably invisible towards the probing radar source. This concept of active RCS reduction has been used to reduce the array RCS of a series-fed linear dipole array using modified improved LMS algorithm. The array performance in terms of active RCS reduction depends upon the geometrical configuration, number of antenna elements, design parameters of radiating element and feed network, and the signal environment considered. It is observed that the current feeding parameter does not affect much the adapted RCS pattern; instead parameters like characteristic and load impedances, power level of probing sources and efficiency of adaptive algorithm play crucial role in placing deep nulls in RCS pattern towards the respective probing sources.

Keywords: Radar cross section, scattering, phased array, center-fed dipole antenna, active cancellation, modified improved LMS algorithm

## 1. Introduction

Defense domain applications demand to design of 'active stealth' based aerodynamic structures. As compared to passive cancellation of scattered power, active RCS reduction is more feasible and practical as it requires less power, and has got cost-effective advantages [1]. The use of modern signal processing components, high-speed microelectronic devices, and phased array techniques have triggered the active stealth technology [2]. The principle behind this active cancellation relies on coherent signal interference where the generated signal cancels the radar echo signals coming from phased arrays mounted over the aerospace structure [1, 2]. The recent development of modern high power extraordinarily sensitive radars with increased detection capability of the low observables that too from a distant range of several kilometers has driven researchers to explore the concept of active RCS reduction. It is a challenge to reduce the RCS without degrading the radiation performance of the antennas.

Recently phased array technique has been employed to realize active RCS reduction using digital radio frequency memory (DRFM), signal processing system unit (SPCU), field programmable gate array (FPGA), and even plasma [3, 4]. The results reported claim improvement in visibility reduction by 20% as compared to other conventional methods [4]. Another novel RCS reduction technique proposed for circularly polarized antenna using etched quasi-fractal slots on the ground plane has shown RCS reduction up to 7.85 dB and 6.95 dB in the band of 1.5 GHz – 10 GHz [5]. Apart from these RCS reduction techniques, implementing bio-inspired algorithms has emerged as a recent trend [6]. These algorithms are capable enough to manipulate the parameters of the antenna array towards optimized performance. As per information available in open domain, enhancement in array performance has been achieved in terms of resonant behavior, directional properties (directivity), antenna gain, polarization pattern, and efficiency. In recent period, improvement in performance of microstrip patch antenna based array has been reported with the help of efficient bio-inspired algorithms like Genetic algorithms (GA), particle swarm optimization (PSO), differential evolution (DE), Invasive weed optimization (IWO) [6]. These algorithms have contributed in achieving dual-band operation with bandwidth enhancement, radiation pattern with symmetrical characteristics and increased gain [7].

In this paper, the concept of active RCS reduction has been used to reduce the array RCS (10 dB or more) of a series-fed linear dipole array using modified improved LMS algorithm for various probing scenarios. The array performance in terms of active RCS reduction depends upon the geometrical configuration, number of antenna elements, dimensions of the dipole, design parameters of radiating element and feed network, and the signal environment considered.

## 2. Theoretical background

For the sake of simplicity, a series-fed linear dipole array is considered here. The array performance in terms of probe suppression depends upon the geometrical arrangement, number of antenna elements, dimensions of the dipole, design parameters of phased array such as inter-element spacing, characteristic and load impedances, the current feeding parameter generated by algorithm, various algorithm parameters and the probing environment considered. These parameters are responsible individually for affecting the array manifold, which is basically the array response towards the impinging signals. For any antenna array, the RCS is a function of the polarization, angle, and frequency of the incident field [8].

### *2.1. Active RCS reduction in a series-fed dipole phased array*

The series-fed linear dipole array considered here is an assembly of center-fed dipole antenna elements placed in a side-by-side configuration. The half-wavelength dipoles are

placed adjacently with common inter element spacing of *d*. The dipole array is excited by a series feed network, consisting of phase shifters, couplers and terminating loads as shown in Figure 1.

The path of the impinging signal once it enters dipole antenna aperture is followed. The individual scattering this signal undergoes at each impedance mismatch within the feed network contributes in total resultant scattered field. The electric field $E_i(\theta,\phi)$ required to compute the overall scattered power, associated with the incident signal is expressed as [9]

$$E_i(\theta,\phi) = f(\theta,\phi)\sum_{i=1}^{N} I_i e^{-j(kd\cos\theta+\alpha)} \tag{1}$$

where $f(\theta,\phi)$ is the radiation pattern of the dipole antenna, $I_i$ is the amplitude excitation, *k* is the wave number and $\alpha$ is the phase excitation respectively.

The radiation pattern for the dipole element is given by

$$f(\theta,\phi) = \frac{j\eta k I_o l e^{-jkr}\cos\theta\left[2\cos(kh\cos\theta)\right]}{4\pi r} \tag{2}$$

where *l, h* are length, and height of the dipole antenna respectively and $I_o$ is a constant. The corresponding radiation pattern of the array can be expressed as

$$|E_i(\theta,\phi)| = |f(\theta,\phi)|.|S| \tag{3}$$

*S* is the steering vector or array response towards the signal incident at an angle of $\theta$. The antenna excitation, $I_i$ in (1) is obtained as antenna weights, using efficient adaptive algorithm, namely modified improved LMS algorithm [2].

The expression for weights calculation $W(m+1)$ considered for a given signal environment is given by [9]

$$W(m+1) = P\left[W(m) - \mu.grad(W(m))\right] + \frac{S}{S^H.S} \tag{4}$$

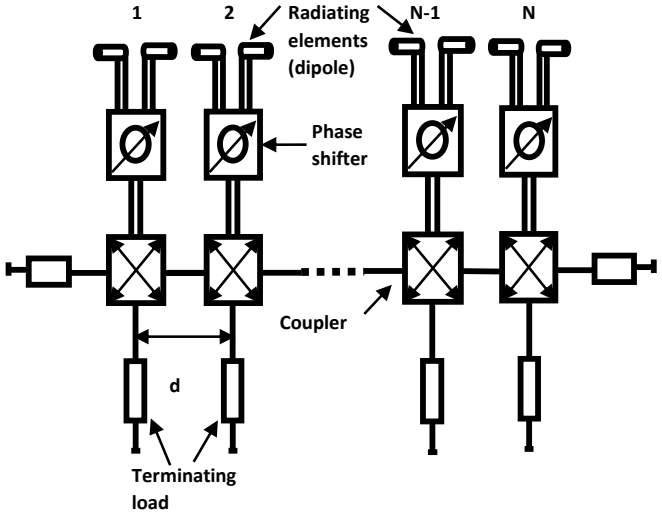


Fig. 1. Schematic of a linear dipole array with series feed network

*P* is the projection operator, *grad* is the gradient vector, *H* denotes Hermitian. The projection vector, *P* is obtained using identity matrix *I* and steering vector as

$$P = I - \frac{S.S^H}{S^H.S} \tag{5}$$

The gradient is obtained using antenna weights and signal covariance matrix $\tilde{R}(m+1)$, mathematically expressed as [9]

$$grad.[W(m)] = 2\tilde{R}(m+1)W(m) \tag{6}$$

$$\tilde{R}(m+1) = \frac{1}{m+1}\left[m\tilde{R}(m) + \hat{R}(m+1)\right] \tag{7}$$

$\tilde{R}(m+1)$ is iteratively updated. The signal covariance matrix $\tilde{R}(m)$ for the received signal $x(m)$ by the *N*-element series-fed linear dipole antenna array is expressed as

$$\tilde{R}(m) = \frac{1}{N}\left[x.x^H\right] \tag{8}$$

The transformed covariance matrix $\hat{R}(m+1)$ used in (7) has the Toeplitz structure [10], and is expressed as

$$\hat{R}(m+1) = \frac{1}{Z}\begin{bmatrix} \hat{r}_o(m+1) & \hat{r}_1(m+1) & \dots & \hat{r}_{M-1}(m+1) \\ \hat{r}_1^*(m+1) & \dots & \dots & . \\ . & \dots & \dots & \hat{r}_1(m+1) \\ \hat{r}_{N-1}^*(m+1) & \dots & \hat{r}_1^*(m+1) & \hat{r}_o(m+1) \end{bmatrix} \tag{9}$$

Here the parameter *Z* is the total antenna impedance of the dipole array consisting of both self and mutual impedances between the antenna elements. The generated total antenna impedance is expressed as

$$Z = \sum_{\substack{x=1 \\ y=1}}^{N} z_{x,y}\,\frac{I_{y,1}}{I_{x,1}} \tag{10}$$

As mentioned above, the optimum antenna weights obtained using modified improved LMS algorithm are used as antenna excitation, $I_i$, a $1\times N$ vector. It is expressed as

$$I_{1\times N} = W(m+1)_{1\times N} \tag{11}$$

Having antenna excitation, radiation pattern and array RCS can be computed for a given phased array including mutual coupling effect. The impedances at different levels of network feed are evaluated starting from the aperture of radiating dipole up till the terminating loads. The overall RCS of the dipole array using the scattered field for the entire dipole array is expressed by [11]

$$\sigma(\theta,\phi) = 4\pi\left|\sum_{n=1}^{N}\left\{\frac{j\eta_o}{4\lambda Z_{rad}}\left(h^2(\cos\theta)\vec{E}_n^r(\theta,\phi)\right)\right\}\right|^2 \tag{12}$$

$$\text{or } \sigma(\theta,\phi) = 4\pi\left|F\sum_{n=1}^{N}\vec{E}_n^r(\theta,\phi)\right|^2 \tag{12a}$$

where $F = \frac{j\eta_o}{4\lambda z_{a_{rad}}}(h)^2 \cos\theta$ (12b)

$N$ being the number of antenna array elements, $\eta$ is the free space impedance, $Z_{rad}$ is the radiation impedance of the antenna array, $h$ is the effective height of the antenna element and $\vec{E}_n^r(\theta,\phi)$ is the total scattered field at the array aperture after being scattered from various impedance mismatches existing within the series feed network. Scattering contributions from different components of the feed network including transmission, reflection, and coupling coefficients are computed further.

The scattered electric field $\vec{E}_{r_n}^r(\theta,\phi)$ due to single radiating element is expressed as [11]

$$\vec{E}_{r_n}^r(\theta,\phi) = r_{r_n} e^{j2(n-1)\alpha} \quad (13a)$$

The corresponding RCS component is obtained by superimposing over all the radiating elements,

$$\sigma_r(\theta,\phi) = F\sum_{n=1}^{N} r_{r_n} e^{j2(n-1)\alpha} \quad (13b)$$

This reflected signal goes back towards the radiating element and thus suffers second-order reflection and transmission. Neglecting the higher order reflections, the scattered field due to $n^{\text{th}}$ phase-shifter is given by

$$\vec{E}_{p_n}^r(\theta,\phi) = t_{r_n}^2 r_{p_n} e^{j2(n-1)\alpha} \quad (13c)$$

The scattered field due to $n^{\text{th}}$ phase-shifter contains the transmitted portion of signal from radiating element to phase shifter. The corresponding RCS component due to phase shifter is obtained by the summation over all the array elements, given as

$$\sigma_p(\theta,\phi) = F\sum_{n=1}^{N} \vec{E}_{p_n}^r(\theta,\phi) \quad (13d)$$

After the signal overcomes the phase shifter, due to $n^{\text{th}}$ coupler, the scattered field is mathematically expressed as

$$\vec{E}_{c_n}^r(\theta,\phi) = (t_{r_n} t_{p_n})^2 r_{c_n} e^{j2(n-1)\zeta} \quad (13e)$$

which in turn generates the overall RCS component due to the scattering at the coupler and is expressed as [11]

$$\sigma_c(\theta,\phi) = F\sum_{n=1}^{N} \vec{E}_{c_n}^r(\theta,\phi) \quad (13f)$$

After undergoing scattering at the coupler level, the signal travels beyond the coupler level towards terminating load. Thus a signal incident at each of the antenna elements move towards the receiving port and subsequently give rise to scattered fields due to forward traveling wave, backward traveling wave, reflection from input load and self-reflection.

The scattered field beyond the coupling port of 4-port lossless couplers is mathematically given by

$$\vec{E}_{s_n}^r(\theta,\phi) = t_{r_n} t_{p_n} r_{l_n} jc_n e^{j(n-1)\zeta} \sum_{m=n+1}^{N} t_{r_m} t_{p_m} jc_m e^{j(m-1)\zeta} \prod_{i=n}^{m-1} t_{c_i} e^{j\psi} + t_{r_n} t_{p_n} jc_n e^{j(n-1)\zeta} \sum_{m=1}^{n-1} t_{r_m} t_{p_m} r_{l_m} jc_m e^{j(m-1)\zeta} \prod_{i=m}^{n-1} t_{c_i} e^{j\psi} + t_{c_n}\left(\vec{E}_{c_n}^t(\theta,\phi)\right) r_{l_n} + r_{in}(jt_{r_n} t_{p_n} c_n)^2 e^{j2(n-1)\zeta} \left(\prod_{i=1}^{n-1} t_{c_i} e^{j\psi}\right)^2 \quad (13g)$$

The corresponding RCS component beyond the coupler level is expressed as [11]

$$\sigma_s(\theta,\phi) = F\sum_{n=1}^{N} \vec{E}_{s_n}^r(\theta,\phi) \quad (13h)$$

The total array RCS is the summation of individual scattered power from all the components, namely radiating antenna elements ($r$), phase shifters ($p$), couplers ($c$) and terminating loads ($s$), expressed as

$$\sigma(\theta,\phi) = 4\pi\left\{\left|\sigma_r(\theta,\phi)\right|^2 + \left|\sigma_p(\theta,\phi)\right|^2 + \left|\sigma_c(\theta,\phi)\right|^2 + \left|\sigma_s(\theta,\phi)\right|^2\right\} \quad (14)$$

The details of analytical formulation may be referred in [10]. The array RCS is adapted as per the given signal scenario with the help of optimum antenna feed currents (weights) obtained using modified improved LMS algorithm. The extent of reduction of RCS value towards probing sources depends on the efficiency of algorithm and its related parameters such as step size, snapshots, available degrees of freedom (DoF). Furthermore, the number of probing sources and their power level also play significant role in RCS reduction. The geometry of antenna elements, the array design parameters decide the structural as well as active RCS of the phased array.

Figure 2 shows a flowchart diagram of active reduction of RCS for a series-fed dipole array. The adapted antenna weights generated using modified improved LMS algorithm are used as current feed to the elements of the dipole phased array for computation of radiation pattern and array RCS.

### *2.2. Impedance analysis*

The parametric analysis towards the objective of achieving active RCS reduction is carried out by varying designing parameters of the dipole array system i.e. characteristic and load impedance for a given signal environment. It has been observed that the achieved RCS reduction towards probing direction is significant when probing is away from array broadside ($0^o$).

Figure 3 shows the trend in variation of null depth at probing angle of -35.60° for distinct values of $Z_O$ and $Z_L$. The range chosen for characteristic impedance ($Z_O$) is 10 Ω to 200 Ω whereas, for load impedance ($Z_L$), it is 10 Ω to 280 Ω.

Table 1 shows the obtained difference in adapted and quiescent RCS for different combinations of array impedances for the probing direction of -35.60°. It may be observed that towards the probing angle of -35.60°, maximum null depth (< -30 dB) can be obtained by having $Z_O$ = 170 Ω and $Z_L$ = 70 Ω.

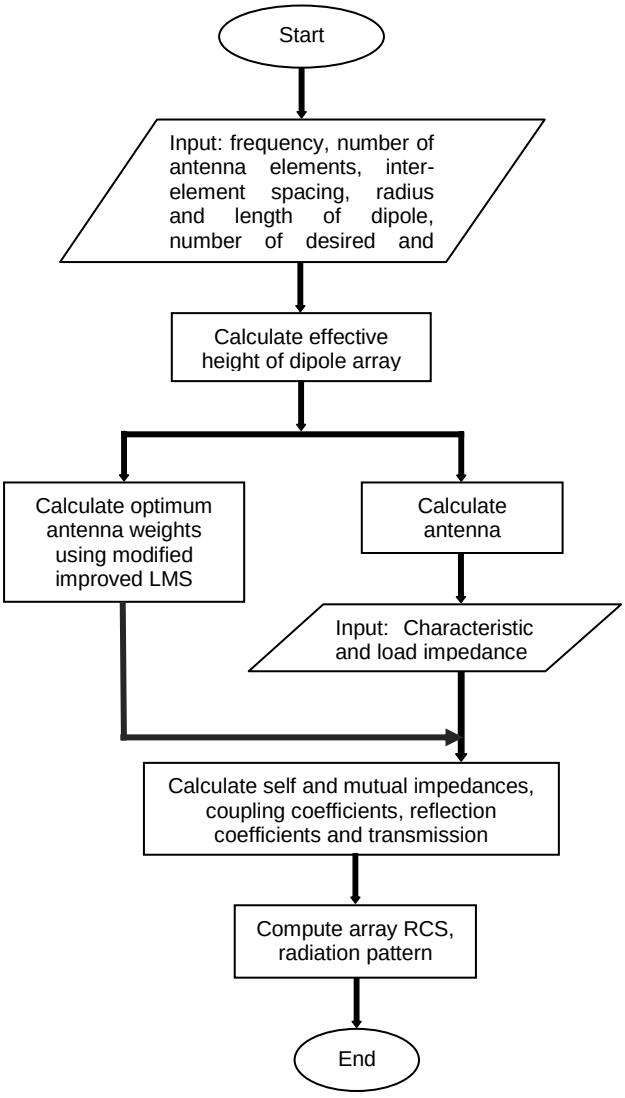


Fig. 2. Flowchart for active RCS reduction in a series-fed dipole

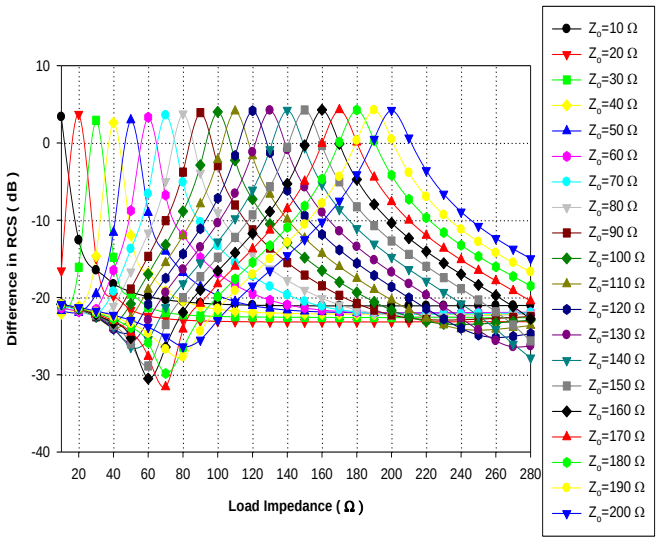


Fig. 3. Difference in adapted and quiescent RCS value at probing angle of -35.60° for different load impedances and characteristic

Table 1. Distinct values of characteristic and load impedances towards probing of -35.60°

| $Z_O$ (Ω) | Difference in adapted and quiescent RCS (dB) | | | | |
|---|---|---|---|---|---|
| | $Z_L$ | | | | |
| | 40 Ω | 50 Ω | 60 Ω | **70 Ω** | 80 Ω |
| 150 | -23.57 | -26.01 | -28.86 | -23.49 | -20.02 |
| 160 | -23.30 | -25.25 | -30.50 | -26.42 | -21.94 |
| **170** | -23.03 | -24.52 | -27.65 | **-31.58** | -24.13 |
| 180 | -22.77 | -23.90 | -25.84 | -29.83 | -26.59 |
| 190 | -22.52 | -23.39 | -24.68 | -26.71 | -27.70 |
| 200 | -22.29 | -22.96 | -23.85 | -25.09 | -26.36 |

Next, further considering the probing cases of 26.80° and 0°, particular values of characteristic and load impedances are identified appropriately only after analyzing the depth of null obtained as the difference between adapted and quiescent RCS values for the mentioned range of array impedances. Apparently, the RCS reduction that can be achieved, is -20 dB approx.) and -5 dB (approx.) towards probing at 26.80° and 0° respectively.

Table 2 summarizes the values of characteristic impedance ($Z_O$), load impedance ($Z_L$) and obtained difference in quiescent and adapted RCS values at probing angles of -35.60°, 26.80° and 0°.

Table 2. Array impedances against various probing angles

| Probe angle | Characteristic impedance, $Z_O$ (Ω) | Load impedance, $Z_L$ (Ω) | Difference in adapted & quiescent RCS (dB) |
|---|---|---|---|
| -35.60° | 170 | 70 | -31.58 |
| 26.80° | 80 | 10 | -20.13 |
| 0° | 185 | 65 | -5.29 |

## 3. Results and discussion

Further, the adapted RCS patterns for multiple signal environments have been compared with the quiescent RCS pattern to analyze the level of RCS reduction towards hostile probing sources positioned at distinct angles. The lobe in broadside direction (0°) is called the specular lobe. It is due to scattering from the aperture of the radiating dipole antenna, phase shifters and inputs of the four port couplers. The other two lobes in the RCS pattern are called input load reflection lobes. The variation of the null depth due to the changes introduced in the designing parameters of the antenna array as well as in probing scenarios is analyzed. The operating frequency is taken as 3 GHz. A 16-element dipole array is considered with series feed network.

### *3.1. Single probing case*

As mentioned earlier, appropriate set of impedances is required for designing low RCS array and achieving active RCS reduction towards the probing direction.

A single probing hostile radar at -35.60° is considered. The power level of probing source is taken as 1000. The characteristic and load impedances are taken 170 Ω and 70 Ω respectively. Using these set of impedances, the generated quiescent RCS pattern (no probing source) impinging the series-fed dipole array, is shown in Figure 4. It may be

observed that a deep null of -31.58 dB in adapted RCS pattern is achieved towards the probing direction of -35.60°. The lobes due to reflections from the input load are nullified at this probing angle. The specular lobe, however, remains with no other distortion in RCS pattern. This deep null makes the array apparently undetectable to the enemy radar attempting to probe at -35.60°.

Next, a probing angle is considered at 26.80°, with the characteristic impedance of 80 Ω and load impedance as 10 Ω. From Figure 5, it is apparent that array RCS got reduced by -20.13 dB at 26.80°. Moreover, there are no additional lobes in the adapted RCS pattern. The efficacy of the algorithm is demonstrated by the deep and accurate nulls obtained at both the input load reflection lobes i.e. at the specified probing angle as well as the direction with no probing source. It may be noted that the adapted RCS patterns obtained for both the probing angles of -35.60° and 26.80° have not shown much distortion as compared to the quiescent RCS pattern. However, if the probing direction matches with the broadside direction of array, this is not the case. The null placement in the specular lobe of RCS pattern will deteriorate the entire RCS pattern with increased level of side-lobes.

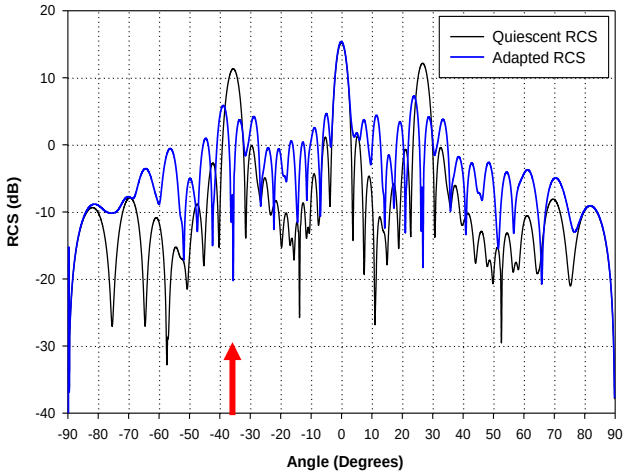


Fig. 4. RCS of a series-fed linear dipole array; $N$ = 16, $d$ = 0.48 λ, $Z_O$ = 170 Ω and $Z_L$ = 70 Ω. One probing source (-35.60°; 1000)

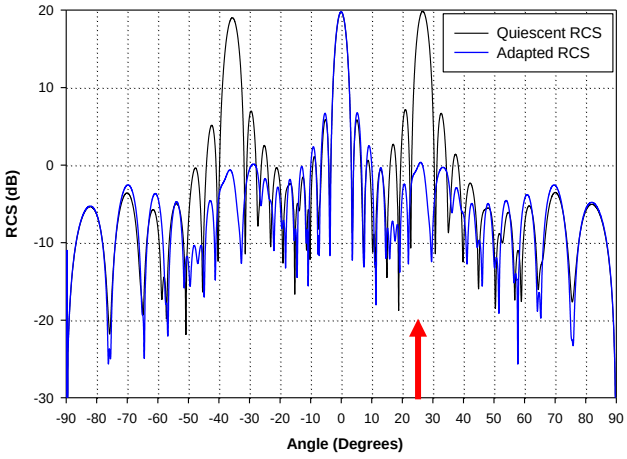


Fig. 5. RCS of a series-fed linear dipole array; $N$ = 16, $d$ = 0.48 λ, $Z_O$ = 80 Ω and $Z_L$= 10 Ω. One probing source (26.80°; 1000)

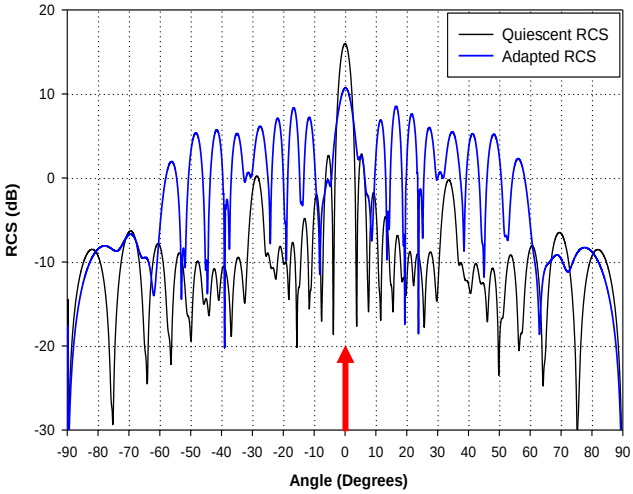


Fig. 6. RCS of a series-fed linear dipole array; $N$ = 16, $d$ = 0.48 λ, $Z_O$ = 185 Ω and $Z_L$ = 65 Ω. One probing source (0°; 1000)

Figure 6 shows that when hostile radar source attempts to probe from 0°, the whole adapted RCS pattern suffers degradation while placing null towards the probing direction (0°). However, the array RCS reduces by -5.3 dB towards the probing source. Here $Z_O$=185 Ω and $Z_L$=65 Ω. This distortion in RCS pattern may be is in accordance with the principle of conservation of energy. The lobe obtained towards specular direction is suppressed well whereas the lobes due to reflections from input loads have shown degradation as shown in the adapted RCS pattern.

### *3.2. Multiple probing case*

It is known that the maximum number of incoming signals any N-element antenna array can handle is N-1. Here as a case of multiple probing, two probing sources are assumed to impinge the dipole array at different angles. The power level of probing sources is varied in the two cases considered.

As a first double probing case (Figure 7a), two probing sources are considered at -36° and 26° with power levels of 50 each. The characteristic and load impedances are taken as $Z_O$ =150 Ω and $Z_L$=225 Ω. It may be observed that RCS is reduced by -21.72 dB and -15.44 dB, placing accurate deep nulls towards the probing sources at -36° and 26° respectively.

For the same set of probing angles i.e., -36° and 26°, but with different power levels (i.e. 1000 each), Figure 7b shows the quiescent and adapted RCS patterns of linear dipole array. It may be observed that RCS reduces by -10.50 dB and -11.14 dB towards probing directions of -36° and 26° respectively. It is apparent from Figure 7a and Figure 7b that both the lobes generated due to reflections from input load are nullified to a great extent at these probing directions.

Figure 8 shows the quiescent and adapted RCS pattern for two probing sources at close angles i.e. -36° and -29° with power level of 1000 each. It is apparent that the RCS value got reduced by -13.88 dB and -16.38 dB at -36° and -29° respectively. The characteristic and load impedances are

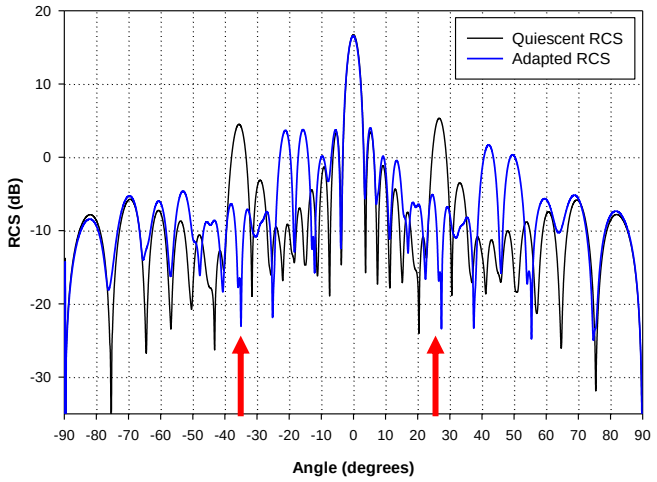


Fig. 7a. RCS of a series-fed linear dipole array; $N$ = 16, $d$ = 0.48 λ, $Z_O$ = 150 Ω and $Z_L$ = 225 Ω. Two probing sources (-36°, 26°; **50**)

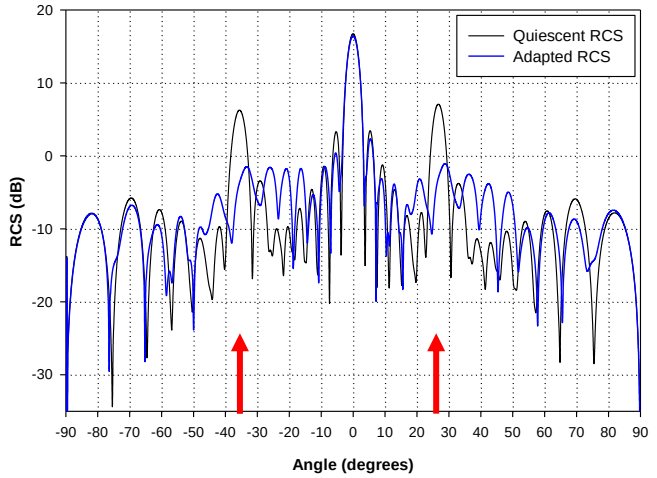


Fig. 7b. RCS of a series-fed linear dipole array; $N$ = 16, $d$ = 0.48 λ, $Z_O$=150 Ω and $Z_L$ =225 Ω. Two probing sources (-36°, 26°; **1000**)

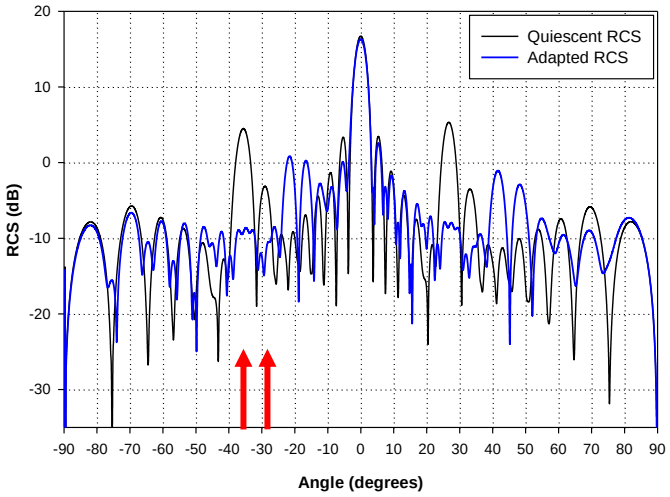


Fig. 8. RCS of a series-fed linear dipole array; $N$ = 16, $d$ = 0.48 λ, $Z_O$ = 150 Ω and $Z_L$ = 225 Ω. Two probing sources (-36°, -29°; **1000**)

taken as $Z_O$ = 150 Ω and $Z_L$ = 225 Ω. It may be observed that there is minimal distortion in adapted RCS pattern even after placement of deep nulls. The equal power level of probing sources makes the weight adaptation slightly complicated. This may result in degenerate Eigen values and Eigen vectors of array correlation matrix, which in turn reduces the array performance in getting optimum weights and hence resultant null depth in RCS pattern.

Further analysis is carried out for the probing case considered in Figure 8 but with different power levels. The power level of 1000 is taken for the probing source placed at -36°. On the other hand, the power level of the source probing at -29° is taken 500. The depth of null obtained at -36° is -13.21 dB whereas against the probing source at -29° is -17.61 dB. It is apparent that the extent of probe suppression is better in this case, as compared to Figure 8. This is as per the expectation lines because of unequal power levels of probing sources. The unequal power level of impinging sources resulted in distinct Eigen values and Eigen vectors of array correlation matrix, and hence better antenna weights. This facilitated the improvement in the array performance in probe suppression.

## 4. Conclusion

The concept of active RCS reduction is successfully employed in a series-fed dipole phased array including mutual coupling effect. The RCS of the dipole array is reduced towards hostile probing direction with the help of efficient modified improved LMS algorithm. The parameters such as array element, its dimension and geometric configuration, frequency of operation, characteristic and load impedances of the array, algorithmic parameters like step size and number of snapshots considered and probing signal environments play important role in controlling array performance in its RCS. The current feeding parameter does not affect much the RCS pattern. This corroborates the efficiency of the adaptive algorithm incorporated for antenna weight adaptation. The values of characteristic and load impedances have eventually shown drastic changes in pattern featuring probe suppression. It is shown that the array is capable of reducing RCS towards the probing directions efficiently. This approach has revealed to be exceptionally efficient in making the aerodynamic structure imperceptible towards hostile radars and thus can be extremely favorable to achieve active stealth in the near future of aerospace applications.

## References

[1] X. Sheng and X. Yuanming, Assemble an active cancellation stealth system, *Defense Electronics Magzine*, vol. 51, no. 7, pp. S16-S22, July 2012.

[2] M.Yi, L.Wang and J.Huang, Active cancellation analysis based on the radar detection probability, *Aerospace Science and Technology*, vol. 46, pp. 273–281, October–November 2015. (doi:10.1016/j.ast.2015.07.018)

[3] P. Yang, F. Yan, F. Yang, and T. Dong, Microstrip phased-array in-band RCS reduction with a random element rotation technique, *IEEE Transactions on Antennas and Propagation*, vol. 64, no. 6, pp. 2513-2518, June 2016.

[4] I. A. Osman and A. A. J. Alzebaidi, Active cancellation system for radar cross section reduction, *International Journal of Education and Research*, vol. 1, No. 7, ISSN: 2201-6740, July 2013.

[5] W. Jiang, T. Hong, and S. X. Gong, Research on the scattering characteristics and the RCS reduction of circularly polarized

microstrip antenna, *International Journal of Antennas and Propagation*, vol. 2013, 9p., 2013. (doi:10.1155/2013/735847)

[6] O. A. Saraereh, A. A. Al Saraira, Q. H. Alsafasfeh and A. Arfoa, Bio-Inspired Algorithms Applied on Microstrip Patch Antennas: a Review, *International Journal on Communication Antenna and Propagation*, vol. 6, No. 6, pp. 336-347, December 2016.

[7] N. Chattoraj and J. S. Roy, Application of Genetic Algorithm to the Optimization of Gain of Magnetized Ferrite Microstrip Antenna, *Engineering Letters*, vol. 14, issue 2, pp. 124-129, 2007.

[8] S. Xu, Y. Xu and J. Huang, The research of active cancellation stealth system design, *Applied Mechanics and Materials*, vol. 192, pp. 390-396, 2012.

[9] H. Singh, N. Bala Ankaiah and R.M. Jha, *Active Cancellation of Probing in Linear Dipole Phased Array*. Springerbrief in Electrical and Computer Engineering-Computational Electromagnetics, ISBN: 978-981-287-828-1, 58 p., 2015.

[10] H. Singh and R.M. Jha, *Active Radar Cross Section Reduction: Theory and Applications*.Cambridge University Press, Cambridge, UK, ISBN: 978-1-107-092617,325 p., 2015.

[11] H. Singh, R. Chandini and R.M. Jha, *RCS Estimation of Linear and Planar Dipole Phased Arrays: Approximate Model*.Springerbrief in Electrical and Computer Engineering-Computational Electromagnetics, ISBN: 978-981-287-753-6, 47 p., 2015.

**Biography of the authors**

Ms Adrija Chowdhury is currently working as Project Scientist in the Centre for Electromagnetics (CEM) of CSIR-National Aerospace Laboratories, Bangalore. She obtained M.Tech. (Optoelectronics &Optical Communication) in 2015 from Amity School of Engineering & Technology, Amity University,Uttar Pradesh. She obtained her B.Tech. (ECE) degree in 2013 from Uttar Pradesh Technical University. She was awarded Prime Minister Scholarship for excellence in academic field for her graduation studies.Her research interests include, radar cross section (RCS) based studies, probe suppression in phased arrays, and active RCS reduction.

Dr R.U. Nair is currently Senior Principal Scientist and Head, Centre for Electromagnetics (CEM), CSIR-National Aerospace Laboratories (CSIR-NAL), Bangalore, India.Ha also holds post of Professor of AcSIR. He received the M.Sc (Physics) and the Ph.D in Physics (Microwave Electronics) from the School of Pure and Applied Physics, Mahatma Gandhi University, Kerala, India, in 1989 and 1997, respectively. During 1992 to 1994, he was a project assistant in the Department of Electronics, Cochin University of Science and Technology (CUSAT), Cochin, Kerala, India. In November 1997, he joined as a lecturer in the Department of Electronics, CUSAT and continued in the same department upto July, 1999. During this period, he participated as a co-researcher in the activities related to international collaborative project for Ground Penetrating Radar (GPR) between CUSAT and International Research Centre for Telecommunications and Radar (IRCTR), TU Delfts, The Netherlands. Dr R U Nair joined CEM, CSIR-NAL in 1999. Dr R U Nair has authored/co-authored over 200 research publications including peer reviewed journal papers, symposium papers and technical reports. He has coauthored a chapter in a book Sensors Update published by Wiley-VCH, Germany, in 2000. The electromagnetic (EM) material characterization techniques developed for his doctoral work were included in the section Perturbation Theory in RF and Microwave Encyclopedia (Vol. 4) published by John-Wiley & Sons, USA in 2005. Dr R U Nair received the CSIR-NAL Excellence in Research Award (2007-2008) for his contributions to the EM design of variable thickness airborne radomes. His research interests include electromagnetic design and performance analysis of radomes, radar cross section, frequency selective surfaces (for Radomes and RAS), EM material characterization, complex media electromagnetics and microwave measurements. He is a life member of Aeronautical Society of India (AeSI), member of ISAMPE and member of IEEE. Dr R U Nair is also an Associate Professor of the Academy of Scientific and Innovative Research (AcSIR), New Delhi.

Dr. Hema Singhis working asPrincipalScientist in Centre for Electromagnetics, National Aerospace Laboratories (CSIR-NAL), Bangalore, India. She also holds post of Associate Professor in CSIR Academy, AcSIR. She received Ph.D. degree in Electronics Engineering from IIT-BHU, Varanasi India in Feb. 2000. For the period 1999-2001, she was Lecturer in Physics at P.G. College, Kashipur, Uttaranchal, India. She was a Lecturer in EEE of Birla Institute of Technology & Science (BITS), Pilani, Rajasthan, India, for the period 2001-2004. She joined CSIR-NAL as Scientist in January 2005.She has been a member of IEEE-Industry Initiative Committee, IEEE, IET, IETE, Indian Society for Advancement of Material and Process Engineering (ISAMPE), and Aeronautical Society of India. Her active areas of research and teaching interests are in the domain of: *Computational Electromagnetics* (CEM) for Aerospace Applications, RF and Microwaves. More specifically, the topics of the sponsored projects she has contributed in are Radar Cross Section (RCS) studies including Active RCS reduction, EM analysis of propagation in an indoor environment, phased antenna arrays, adaptive array processing, and conformal array. Dr. Singh has authored or co-authored 11 books, 1 book chapter, 7 software copyrights, 235 scientific research papers and technical reports. She has also supervised over 40 graduate projects and postgraduate dissertations.Dr. Hema Singh received Best Woman Scientist Award in NAL, Bangalore for period of 2007-2008 for her contribution in area of phased antenna array, adaptive arrays, and active RCS reduction.